Synthesis and study of novel multifunctional cyclodextrin-deferasirox hybrids

Article (Accepted Version)

FULL PAPER

Synthesis and Study of Novel Multifunctional Cyclodextrin-Deferasirox Hybrids

Jose Miguel Gascon,[a] Valentina Oliveri,[a,b]* Andrew McGown,[a] Ecem Kaya,[c] Yu-Lin Chen,[d] Carol Austin,[e] Martin Walker,[e] Frances M. Platt,[c]* Graziella Vecchio,[b]* and John Spencer, [a],*

Abstract: Metal dyshomeostasis is central to a number of disorders that result from, *inter alia*, oxidative stress protein misfolding, and cholesterol dyshomeostasis. In this respect, metal deficiencies are usually readily corrected by treatment with supplements, whereas metal overload can be overcome by the use of metal-selective chelation therapy. Deferasirox, 4-[(3*Z*,5*E*)-3,5-bis(6-oxo-1-cyclohexa-2,4-dienylidene)-1,2,4-triazolidin-1-yl]benzoic acid, Exjade, or ICL670, is used clinically to treat hemosiderosis (iron overload), which often results from multiple blood transfusions. Cyclodextrins are cyclic glucose units that are extensively used in the pharmaceutical industry as formulating agents as well as for encapsulating hydrophobic molecules such as in the treatment of Niemann Pick C or for hypervitaminosis. We have conjugated deferasirox, via an amide coupling reaction, to both 6^A-amino-6^A-deoxy-β-cyclodextrin and 3^A-amino-3^A-deoxy-2^A(S),3^A(S)-β-cyclodextrin, at the upper and lower rim respectively creating hybrid molecules with dual properties, capable of both metal chelation and cholesterol encapsulation. Our findings emphasize the importance of the conjugation of β-cyclodextrin with deferasirox to significantly improve the biological properties and reduce the cytotoxicity of this drug.

Introduction

Chelation therapy is considered as one treatment option to reduce the toxic effects of metal ions in humans. Besides the removal of toxic foreign metals, chelation therapy is also used to reduce levels of essential metals in cases of copper or iron overload disorders as in Wilson's disease, primary and secondary hemochromatosis.[1,2] Moreover, the use of chelating agents has also been proposed for neurodegenerative disorders related to oxidative stress, disruption of metal, and cholesterol homeostasis.[3,4] Deferasirox (**3**, Exjade, ICL670) is an orally available, once-daily, clinical iron chelator commonly used to treat hemosiderosis, after multiple transfusions, non–transfusion-dependent thalassemia (NTDT), sickle cell anemia and myelodysplastic syndromes (MDS).[5] The development of chelating agents for iron, which, nowadays includes desferal, deferiprone and deferasirox, is challenging given that all present different drawbacks.[6-8] In particular, nephrotoxicity is one of the most frequent adverse effects of iron chelator treatment.[9]

In an attempt to overcome these limitations, different strategies have been proposed, viz. covalent modification of the deferasirox scaffold[10] and non-covalent inclusion in a cyclodextrin (CyD) cavity.[11]

We have previously conjugated metal chelators such as deferiprone and clioquinol with β-cyclodextrin (CyD).[12,13] Studies on these conjugates have indicated that the CyD conjugation improves some features of chelators and makes them multifunctional.[14,15] CyDs have been studied as artificial chaperones and antiaggregant agents.[16,17] Methyl-β-CyD has been reported to reduce α-synuclein (αSyn) accumulation, a protein implicated in Parkinson's disease (PD).[18] Also, some authors have reported that dietary CyDs can influence metallothionein mRNA levels in rats.[19] This ability may cooperate with the chelating ability of the moiety since metallothioneins play a prominent role in metal homeostasis. Finally, the CyD cavity can be available to include exogenous drugs as well as endogenous cholesterol and lipids that are also involved in neurodegenerative diseases. Several studies have investigated the effect of cholesterol-reducing agents such as CyDs on neurodegenerative pathologies.[20,21] Trappsol TM, hydroxypropyl-beta-cyclodextrin (HP-B-CD), is currently under clinical trials in Niemann–Pick type C (NPC), a lysosomal lipid storage disorder characterized by an accumulation of lipids such as cholesterol. This context has inspired us to synthesize and investigate new conjugates of CyD with deferasirox. Herein, we report the synthesis and characterization of 4-[3,5bis(2-hydroxyphenyl)-1H-1,2,4triazol-1-yl]-N-[6^A-amino-6^A-deoxy- β -cyclodextrin]-benzamide (**1**, Figure 1) and 4-[3,5-bis(2-hydroxyphenyl)-1H-1,2,4-triazol-1-yl]-N-[3^A-deoxy-3^A-amino-β-cyclodextrin]-benzamide (**2**, Figure 1) since 3- and 6-monofunctionalized β-cyclodextrin may have significant different chemical and biological properties owing to their different structures. Given the multifactorial nature of neurodegenerative

[a] Dr. J. M. Gascon, Dr. V. Oliveri, Dr A. McGown, Prof J. Spencer
Department of Chemistry
School of Life Sciences, University of Sussex
Falmer, Brighton, East Sussex BN1 9QJ, UK
E-mail: valentina.oliveri@unict.it ; J.Spencer@sussex.ac.uk
[b] Dr. V. Oliveri, Prof. G. Vecchio
Dipartimento di Scienze Chimiche
Università degli Studi di Catania
Viale A. Doria 6, 95125 Catania, Italy
E-mail: gr.vecchio@unict.it
[c] Miss E. Kaya, Prof. F. Platt
Department of Pharmacology
University of Oxford
Mansfield Road, Oxford OX1 3QT, UK
E-mail: frances.platt@pharm.ox.ac.uk
[d] Dr. Y.-L. Chen
Pharmaceutical Science
King's College London
Franklin Wilkins Building, London, SE1 9NH, UK
[e] Dr. C. Austin, Dr. M. Walker
Eurofins Selcia Drug Discovery
Fyfield Business & Research Park
Fyfield Road, Ongar, Essex CM5 0GS, UK

Supporting information for this article is given via a link at the end of the document.

disorders, we evaluated the ability of the new CyD conjugates to act on multiple targets. Hence, we studied the antioxidant activity of the deferasirox conjugates, the stability of their iron(III) complexes, and the ability to inhibit metal induced αSyn aggregation. We also evaluated the cytotoxicity of **1** and **2** in vitro and their effects in NPC cell models. Deferasirox (**3**) was also investigated for comparative purposes. The chemical and biological properties of the conjugates confirm that the conjugation with the CyD cavity represents a promising strategy to design new non-toxic multifunctional molecules.

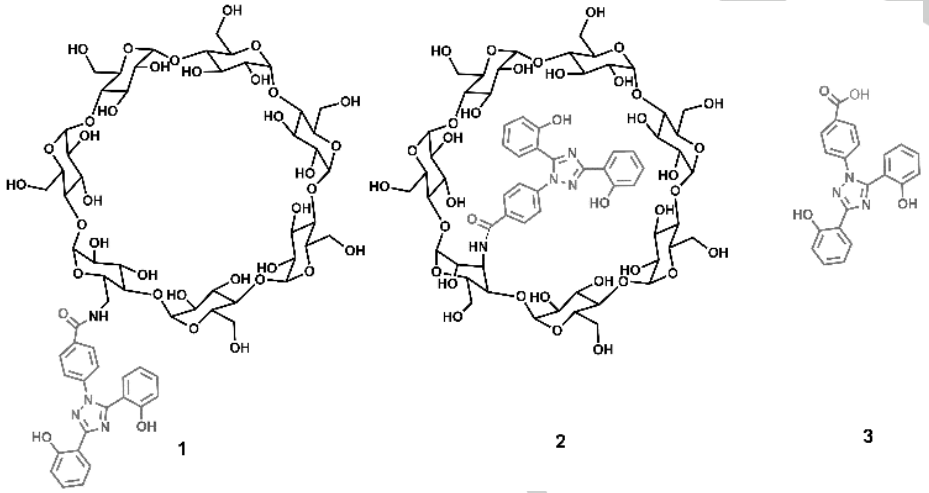

Figure 1. Chemical structure of the derivatives in this study.

Results and Discussion

Synthesis and Characterization

Considering the pharmacological properties of **3** and the ability of CyDs to act as carriers, antiaggregants, and neuroprotective agents, we envisaged a simple reaction via the carboxylic group of **3** to obtain novel CyD conjugates. Amide condensation was thus performed between **3** and 6^A-amino-6^A-deoxy-β-cyclodextrin or 3^A-amino-3^A-deoxy-2^A(S),3^A(S)-β-cyclodextrin in the presence of suitable activating agents to obtain the 6-monofunctionalized **1** and the 3-monofunctionalized **2** isomers, respectively.

Such conjugation was confirmed by mass spectrometry (MS). ESI-MS spectra of the conjugates **2** and **1** show two peaks resulting from singly charged (*m/z* 1511.4 $[P+Na]^+$) and doubly charged ions (*m/z* 764.2 $[P+H+K]^{2+}$). 6-Functionalized and 3-functionalized derivatives have significant differences due to the different synthetic routes followed to obtain the amino-CyD used in the amide condensation reaction. Because of a chair flip of the modified altrose unit in the 3-functionalized CyD derivatives, the cavity is elliptically distorted, whereas the functionalization at the 6-position does not dramatically influence the CyD cavity according to the literature.[22,23] Thus, the kind of functionalization strategy used to obtain the CyD conjugates may confer different properties to the resulting conjugates.[24]

The new compounds were further characterized by ^{1}H and ^{13}C NMR spectroscopy. The 1D spectra of the products were assigned using 2D experiments (COSY, TOCSY, HSQC, HMBC, and ROESY, Figures S1-S6). The NMR spectra of **1** and **2** further confirm ligand conjugation as they display signals due to the **3** and CyD moieties, the former resonating in the aromatic region. Other diagnostic signals of these CyD conjugates include those of the carbonyl groups at δ=166.0 and 165.4 ppm in the ^{13}C spectrum of **1** and **2**, respectively.

As for **1**, chemical shifts corresponding to H-1 protons (Hs-1) of the CyD moiety are divided into four groups (Figure 2) upon the functionalization that made them inequivalent. Moreover, H-6 protons (Hs-6) of the CyDs are spread as a consequence of the presence of the aromatic moiety linked to the CyD rim. In particular, the H-6A protons appear at **δ**= 4.05 and 3.04 ppm because of the aromatic ring current effect as reported for other aromatic CyD derivatives.[25]

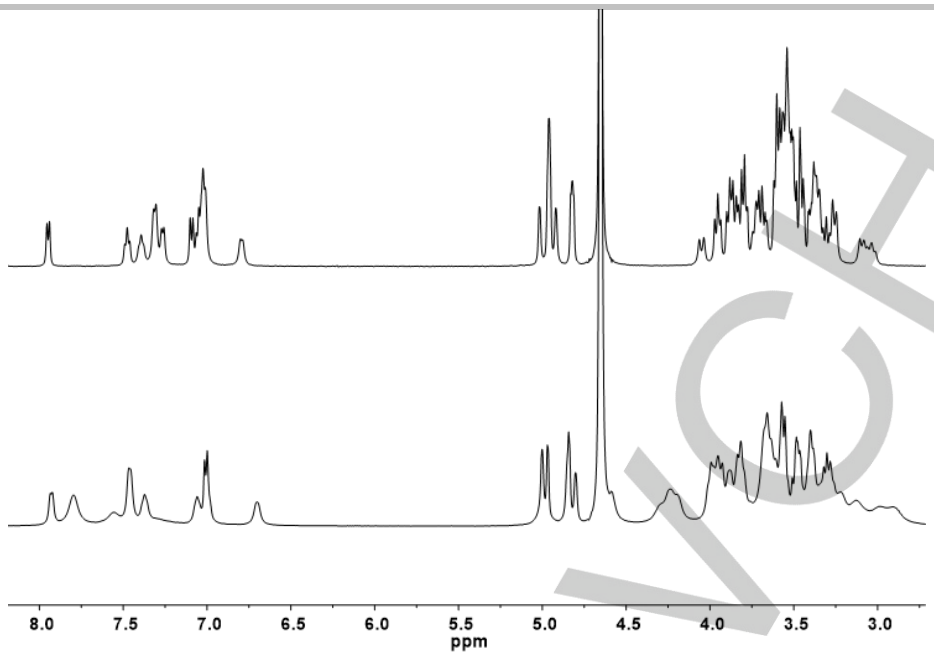

Figure 2. ^{1}H NMR spectra of **1** (top) and **2** (bottom) in D_2O at 500 MHz..

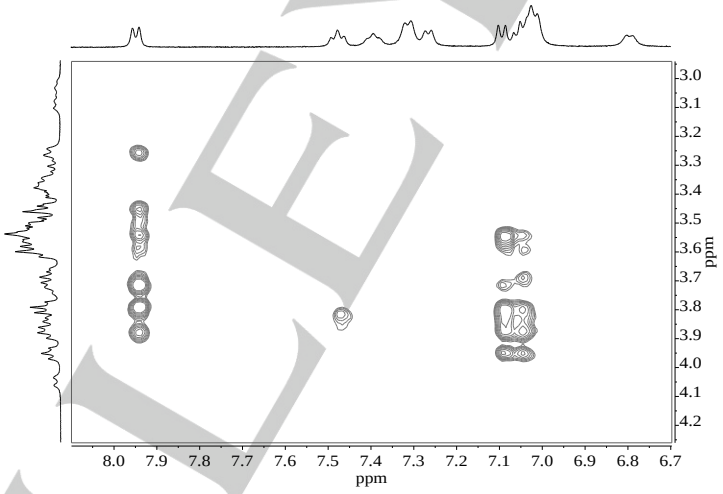

Figure 3. ROESY spectrum of **1** in D_2O at 500 MHz.

The analysis of the ROESY spectrum (Figure 3) reveals the presence of through-space proximities between an aromatic ring of the **3** moiety and Hs-3, Hs-5 of the CyD. Since these protons of the CyD are pointed towards the interior of the cavity, the formation of an inclusion complex of the pendant with the CyD cavity can be hypothesized. In particular, intense cross peaks were detected between H-13, H-14, H-15, and H-16 of the aromatic ring **a** and Hs-3 and Hs-5 of the CyD. ROESY data suggest that the phenolic ring **a** is inside the CyD cavity.

Moreover, the NMR spectrum did not change with the increase of the concentration of **1** suggesting the intramolecular interaction and, therefore, the self-inclusion of the pendant. This compound was also characterized by CD spectroscopy in order to further investigate the interaction of the **3** moiety with the β-CyD cavity. The CD spectrum, at pH 6.8, of **1** shows two positive bands at 211 and 315 nm and two more intense negative bands at 233 nm and 275 nm. These bands are in the absorption region of the aromatic rings and are due to the dipole-dipole coupling between the **3** moiety and the β-CyD cavity. This behavior has been generally reported for functionalized CyDs, and it is due to the interaction of

the functionalizing moiety[26] with the CyD. Furthermore, the CD spectrum is strongly influenced by the presence of 1-adamantanol (ADM), a well-known high-affinity guest of CyD cavity, in keeping with the self-inclusion (Figures 4 and S7). The intensity and absorption maximum wavelength of the band's changes with increasing concentrations of ADM suggesting a modification of the orientation of the aromatic pendant concerning the CyD cavity.

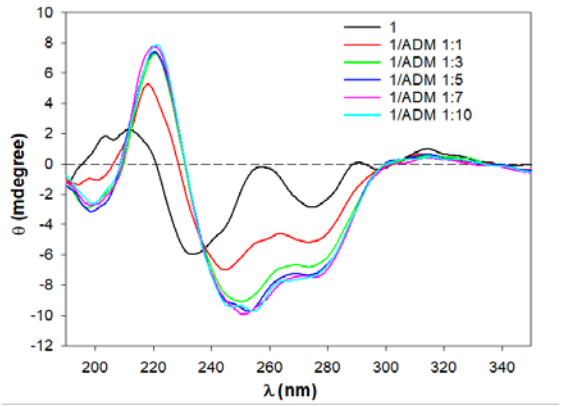

Figure 4. CD spectra of **1** (50 µM) in the presence of increasing concentrations of ADM (50-500 µM).

Analogously to **1**, the self-inclusion of the aromatic ring **a** can be proposed for the 3-functionalized conjugate by NMR and CD data. The ^{1}H NMR spectrum of **2** shows that the functionalization splits out the H-1 protons of the CyD into five groups (Figure 2). In particular, H-1A of the functionalized sugar of the CyD resonates at 4.58 ppm. The synthetic strategy followed to functionalize CyDs at the 3-hydroxyl group leads to configuration inversions of C-2 and C-3 and an altrose unit (ring A) replaces a glucose unit in the CyD molecule (Figure S8). As a consequence, H-2A and H-3A are strongly shifted downfield at 4.30 ppm as typically observed for other 3-functionalized derivatives.[19] ROESY spectra display intense NOE-correlation peaks between aromatic protons and inner CyD protons suggesting the inclusion of ring **a** (Figures S9 and S10).

Finally, further evidence of the self-inclusion of the pendant is provided by CD experiments (Figure 5) in the presence of ADM. CD spectra of **2** show intense dichroic bands at 222, 233, 275 and 315 nm. These bands are associated with the π- π* absorption bands of the aromatic moiety. The differences in CD spectra of **1** and **2** can be anticipated according to the empirical rules that interpret the induced circular dichroism observed for a chromophore inside or outside of the CyD cavity.[26] **1** and **2** are structural isomers, and the rim of **2** is quite distorted owing to the presence of the altrose ring. For this reason, a different orientation of the 3 moiety in **1** and **2** can explain the different CD spectra.

The reduction in the intensity of the dichroic bands of **2** with increasing concentrations of ADM reveals the displacement of the included aromatic ring from the CyD cavity (Figure 5).

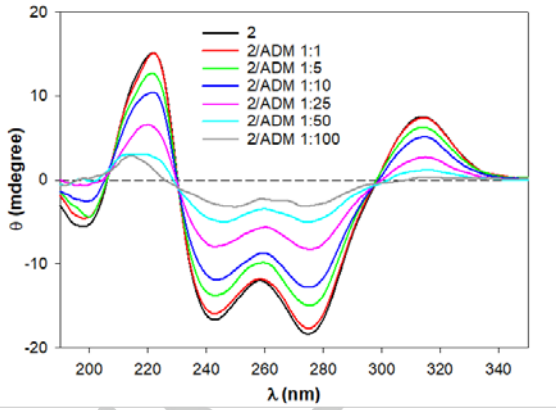

Figure 5. CD spectra of **2** (50 µM) in the presence of increasing concentrations of ADM (50 µM-5 mM).

Proton and iron(III) complex stability constants

Ligand **3** possesses a 1,2,4-triazole framework substituted by two phenolic substituents in position 3 and 5 and a benzoic acid moiety in position 1. The values of proton/iron(III) stability constants were determined by spectrophotometric titrations (Figures S11-S19) and are reported in Tables 1 and 2.

For protonation stability constants (Table 1), $pK_{a\text{-carboxy}}$ corresponds to the deprotonation of the carboxylic group, whereas the values of $pK_{a\text{-phenol1}}$ and $pK_{a\text{-phenol2}}$ are characteristic of the deprotonation of the phenolic groups. The values determined in this study are consistent with the values reported elsewhere.[27]

In comparison with **3**, both CyD compounds **1** and **2** possess lower pK_a values associated with the deprotonation of phenolic groups. NMR and CD data suggest the self-inclusion of the **a** ring of the CyD derivatives and this behavior could decrease the protonation constant of this phenol group compared to **3**. A decrease in the values of the protonation stability constants has been reported in the literature for other CyD derivatives and has been attributed to the hydrophobic effects of the CyD cavity.[12]

Table 1. pK_a values for **3** and the two conjugates (25°C, 0.1 M KCl) in the molar ratio of 1:0.2 H_2O/DMSO solution. Repeated measurements can result in about 3% error.

pK_a	3	1	2
$pK_{a\text{-carboxy}}$	4.8	-	-
$pK_{a\text{-phenol1}}$	10.3	8.8	9.5
$pK_{a\text{-phenol2}}$	12.3	12.1	12.0

For iron(III) stability constants, **3** is a tridentate chelating agent, mainly forming a 2:1 chelator/iron(III) complex at physiological pH.[28] Our data (Table 2) confirm these results and demonstrate that the CyD conjugates form the FeL and FeL_2 species similarly to **3**. In particular, FeL_2 is the sole complex species present at physiological pH for both CyD conjugates (Figures S14 and S19; pH 8.4 in the molar ratio of 1:0.2 H_2O/DMSO solution is closely equivalent to pH 7.4 in the aqueous solution). However, the iron(III) complex stability constants values of **1** and **2** are lower than those of **3**. This trend has been observed for other CyD derivatives and associated to the steric hindrance associated with the CyD scaffold.

Table 2. Overall formation constants (log βmnq) of Fe^{III} complexes with 3 and the two conjugates (25 °C, 0.1 M KCl) in the molar ratio of 1:0.2 H_2O/DMSO solution. Repeated measurements can result in about 3% error.

log β_{mnq}	3	1	2
log β_{111}	27.0	-	-
log β_{110}	24.5	21.4	21.8
log β_{121}	45.3	-	-
log β_{120}	39.3	35.3	36.0
*$pFe^{III}_{8.4}$	23.6	22.5	22.7

*pFe^{III}8.4 were calculated under the conditions of $[Fe^{III}]_{total}$ =1 μM, $[ligand]_{total}$=10 μM and pH=8.4. pH 8.4 in the molar ratio of 1:0.2 H_2O/DMSO solution is closely equivalent to pH 7.4 in the aqueous solution.

Antioxidant activity

Mounting evidence suggests a pivotal role of oxidative stress in metal-overload diseases[29] and neurodegenerative diseases[30] and hence much effort has been undertaken to target it using new and powerful antioxidants.[31] Antioxidants such as polyphenols, vitamins A and E have been proposed as therapeutic agents for preventing and reducing the rate of progression of neurodegenerative diseases.[32]

To assess the antioxidant activity of the CyD derivatives, the Trolox equivalent antioxidant capacity (TEAC) assay was used to quantify it.

The capacity of the systems to scavenge $ABTS^{\bullet+}$ at 1, 3, and 6 minutes was compared to Trolox, an analog of vitamin E, and was thus expressed as TEAC values (Figure 6). The antioxidant activity of **1** is two times higher than Trolox and similar to that of **3**. Furthermore, it increases in a time-dependent manner; on the other hand, the TEAC values of **2** are slightly lower than those of **1** and **3**. These data suggest that the free radical scavenging capacity of the derivatives can be attributed to the high reactivity of the hydroxyl groups on the aromatic rings as observed for other analogous systems.[19] In the case of **2**, the hydroxyl groups may be less available to react with the radical cation, probably due to the higher rigidity of the system compared to the analogous 6-functionalized derivative. Similar behavior has also been reported for related cyclodextrin-deferiprone conjugates.[12] However, the ability of **2** to scavenge free radicals is much higher than that of Trolox. This suggests that the CyD conjugates could be powerful antioxidants with activity similar to that of several polyphenols.

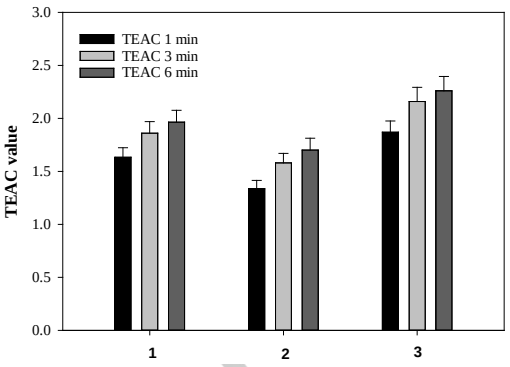

Figure 6. TEAC values at 1, 3, and 6 min for CyD derivatives **1**, **2,** and **3**. The values are expressed as the average of three independent assays, and error bars show standard deviations.

Effect on α-synuclein aggregation

The aggregation of proteins into toxic conformations plays a critical role in the development of different neurodegenerative disorders such as PD, Alzheimer's diseases (AD), and dementia with Lewy Bodies (DLB).[33]

DLB and PD are amongst a group of diseases referred to as α-synucleinopathies that are characterized by α-synuclein (αSyn) accumulation in cortical and subcortical regions.[34] Therefore, compounds that can delay and/or prevent the aggregation process of αSyn could lead to a new therapeutic strategy for treating PD and other α-synucleinopathies. The interaction of proteins with metals often plays a crucial role in the aggregation. In particular, copper(II) and iron(III) are the most effective ions in promoting αSyn aggregation.[35]

To investigate the influence of both CyD conjugates (**1** and **2**) on αSyn aggregation, we monitored the iron and copper-induced fibrillation of the protein in the absence and presence of **1**, **2** and their parent compounds (**3** and βCyD) using a dynamic light scattering (DLS) technique. The effect of **3** on the metal-induced αSyn aggregation was not determined because of the precipitation of its metal complexes in the assay conditions.

The hydrodynamic diameter of αSyn (mean diameter = 6.4 ± 0.3 nm) confirms the existence of the protein in a monomeric state in keeping with data reported elsewhere.[36,37] Moreover, the size distribution of αSyn remains substantially unchanged after 24 h in these conditions. The presence of Fe^{3+} and Cu^{2+} promotes aggregate formation.

DLS data indicate that both CD conjugates **1** and **2** efficiently inhibit metal-induced αSyn aggregation whereas unfunctionalized β-CyD was not able to suppress the aggregation. In particular, **1** prevents αSyn aggregation at *t*=0 and shows only a small percentage of oligomers (5 %) with a mean diameter of 28 nm at *t* = 24 h (Figure S20). Analogously, **2** is efficient in suppressing αSyn aggregation (Figure S21). Indeed, no aggregate is discernible at *t* = 0 and *t* = 24 h, only the size distribution (i.e., the polydispersity index) of the protein increased to a small extent. The behavior of these derivatives could be explained by the correlation between the capacity of inhibiting metal-induced aggregation and their metal-binding ability. As described above, **1**, **2,** and **3** form a 2:1 chelator/iron complex at physiological pH with high stability constant.[27,28] **3** also has a moderate affinity for Cu^{2+} as demonstrated by the value of 18.8 for log β (CuL), and 23.9 for log β_2 (CuL_2) reported elsewhere.[38] As observed for iron, we anticipate the conjugation with CyD does not significantly modify the copper-binding ability of the chelators.[12,31] Moreover, we confirmed through UV-vis and CD spectroscopy that both derivatives maintain the ability of **3** to complex copper ions. In particular, the absorption and CD bands of both CyD conjugates dramatically change upon addition of Cu^{2+} ions indicating the copper complexation (Figure S22). Overall, these systems can be used to gain control of iron and copper toxicity that is strictly implicated in protein aggregation.

Effect on Niemann-Pick disease type C (NPC) Cells

Since CyDs are applied in NPC, and other neurodegenerative disorders and CyD treatment has been shown to be beneficial and well-tolerated in NPC cells, we tested **3** and its CyD conjugates (**1** and **2**) in NPC cells in comparison with HP-B-CD. For completeness, we also evaluated the known compound **4** (a dual

action CyD-Cu chelator)[12] and the clioquinol-like CyD analog **5** (Figure S23) that belong to a class of CyDs conjugates formerly proposed by us as multifunctional antineurodegenerative agents. A dose-response study was performed on *Npc1*$^{+/+}$ (wild type) CHO cells using 72 hours of treatment to determine the cytotoxicity profiles. CyD compounds did not have any detrimental effects in terms of cell viability and did not affect relative lysosomal volume in the concentrations range tested (Figure 7). The conjugation with CyD significantly reduced the cytotoxicity of these compounds as observed in the case of other CyD conjugates.[39] However, treatment with **3** over 72 hours significantly reduced viability at all doses tested, compared to the untreated group and CyD treated cells in a dose-dependent dependent manner (Figure 7A). Also, **3** increased the acidic compartment volume of *Npc1*$^{+/+}$ CHO cells at low concentrations (55% at 50 μM, 35% at 100 μM) in WT cells, while decreasing total acidic compartment volume at high concentrations (39% at 250 μM, 69% at 500 μM) (Figure 7B).

These compounds were then tested on NPC1 deficient CHO cells. *Npc1*$^{-/-}$ cells showed substantial increase in relative lysosomal volume (32%) compared to *Npc1*$^{+/+}$ cells (p<0.0001) (Figure 7C).

Total acidic compartment volume decreased with **4** by 21.5% (p<0.0001-normalised to *Npc1*$^{+/+}$ levels with p 0.0539), with **1** by 23.5% (p<0.0001), **2** by 20.3% (p<0.0001), **5** by 12.3% (p<0.001), HPBCyD by 30% (p<0.0001-normalised to *Npc1*$^{+/+}$ levels p value 0.9995) and **3** by 23.5% (p<0.0001 normalised to *Npc1*$^{+/+}$ levels with p 0.0534) (Figure 7C).

A toxicity study (Table 3) in HepG2 (immortalized human liver carcinoma cells) was carried out. This confirmed that the CyD-deferasirox conjugates **1**, **2** are substantially less toxic (or less antiproliferative) *in cells* than deferasirox alone (Figure S24). Solubility studies established that **1**-**3** had good solubility (>100 μM (Table S1).

Table 3. HepG2 toxicity study.

Compound	IC_{50} (μM)[a]
1	>100
2	>100
3	0.98[b]

[a] (average of 3 replicates). [b] estimated.

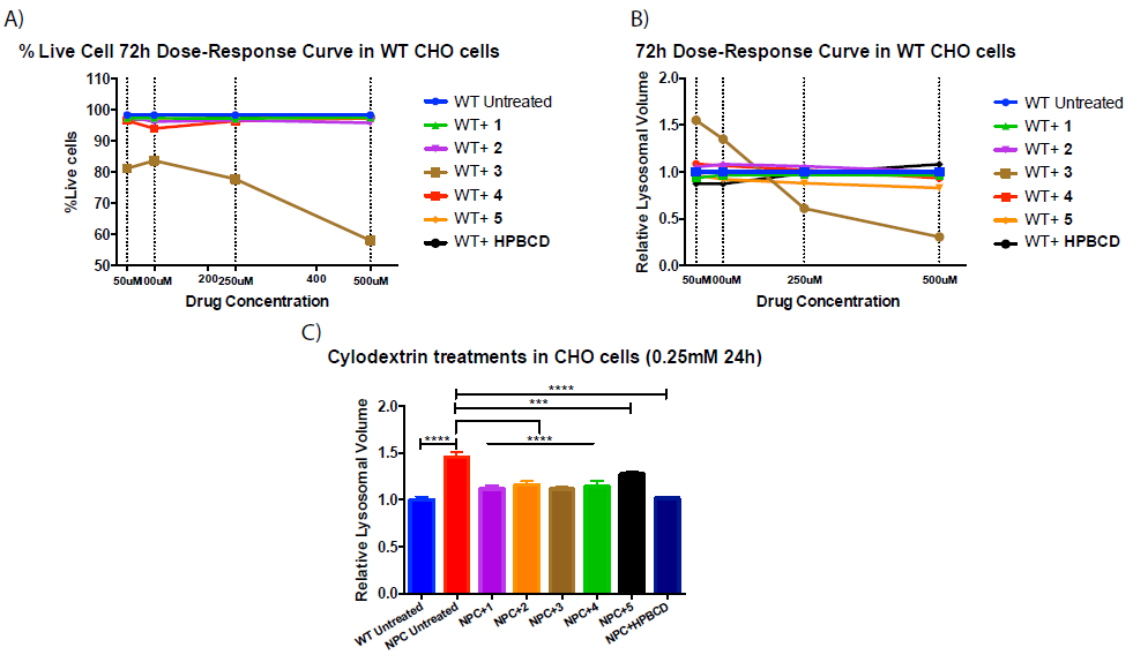

Figure 7. Effect of CyDs on NPC cells.

Conclusions

Two novel CyD-conjugated deferasirox analogs, **1** and **2**, have been synthesized and thoroughly investigated. The derivatives have significant in vitro antioxidant capacity and can complex metal ions with high stability constants. Therefore, they can completely inhibit metal-induced protein aggregation and the formation of amyloid fibrils. These features of **1** and **2** are highly desirable considering the critical involvement of metal ions in protein misfolding and aggregation, which are hallmarks of several neurodegenerative disorders.

Furthermore, the cyclodextrin moiety renders these systems less toxic than deferasirox, well-known for the side effects when administrated in iron-overload diseases. Most important advantages of both **1** and **2** are their good solubility in water and the possibility of forming inclusion complexes to include

endogenous compounds, such as cholesterol, correcting lysosomal volume in NPC cells. Compared to the other CyD conjugates previously studied by us,[12,13] **1** and **2** represent the first example of non toxic conjugates of a drug on the market that we have studied in a model of Childhood Alzheimer's (NPC). Overall, the conjugates hold promise as multitargeted therapies in the treatment of disorders of metal dyshomeostasis and lipid imbalances.

Experimental Section

Chemicals

6^A-Amino-6^A-deoxy-β-cyclodextrin was synthesized by a microwave-assisted procedure starting from the corresponding 6-tosylate derivative as reported elsewhere[40], whereas 3^A-amino-3^A-deoxy-2^A(S),3^A(S)-β-cyclodextrin was obtained from TCI. Starting materials were purchased from Molekula, UK or Cyclolab, Hungary, and human αSyn was purchased from Sigma–Aldrich. Cu^{2+} stock solutions were prepared by dissolving the corresponding perchlorate in water and titrating the resulting solutions with standardized EDTA by using murexide. Ferric ion solutions were prepared by dissolving $FeCl_3 \cdot 6H_2O$ in 0.01 M hydrochloric acid to prevent hydrolysis. Iron solution titer was spectrophotometrically determined on the Fe–desferal complex at 428 nm. For clarity, the sugar units in β-CyD derivatives are labeled A–G counter-clockwise starting from the modified ring (denoted as A) and viewing from the upper rim (Figure S25).

*Synthesis of 4-[3,5bis(2-hydroxyphenyl)-1H-1,2,4-triazol-1-yl]-N-[6^A-amino-6^A-deoxy-β-cyclodextrin] benzamide (**1**)*

HOBt (24 mg, 0.175 mmol), DCC (36 mg, 0.175 mmol) and triethylamine (50 µL, 0.53 mmol) were added to a solution of **3** (65.5 mg, 0.175 mmol) in dry DMF (5 mL). After 20 min, 6^A-amino-6^A-deoxy-β-cyclodextrin (205 mg, 0.175 mmol) was added. The reaction was stirred at room temperature under argon for 48 h. The solvent was evaporated to dryness in vacuo. The crude product was then triturated with diethyl ether (3 × 3 mL), followed by an acetone trituration cold (3 × 4 mL) and hot acetone trituration (3 × 3 mL) and the crude solids were purified by reverse phase chromatography using a 30g Biotage KP-RC-18 column (eluent: $H_2O \rightarrow CH_3OH$) to give the title product (white solid). For numbering of **1** refer to Figure 1. Yield: 64 % (168 mg, 0.11 mmol); TLC: Rf=0.28 (iPrOH/AcOEt/H_2O/NH_3 4:3:2:1); ^{1}H NMR (500 MHz, D_2O): δ 7.95 (d, $J_{13,14}$ = 7.7 Hz, 1H, H-13), 7.48 (t, J = 7.8 Hz, 1H, H-15), 7.39 (m, 1H, H-21), 7.31 (d, $J_{8,7} = J_{10,11}$ = 8.0 Hz, 2H, H-8 and H-10), 7.26 (d, $J_{23,22}$ = 7.5 Hz, 1H, H-23), 7.09 (d, $J_{16,15}$ = 8.2 Hz, 1H, H-16), 7.04 (m, 4H, H-7, H-11, H-14 and H-22), 6.79 (d, $J_{20,21}$ = 7.8 Hz, 1H, H-20), 5.02 (d, $J_{1G,2G}$ = 3.6 Hz, 1H, H-1G of CyD), 4.96 (d, J = 3.5 Hz, 3H, Hs-1 of CyD), 4.92 (d, J = 3.6 Hz, 1H, H-1A of CyD), 4.82 (d, J = 3.6 Hz, 2H, Hs-1 of CyD), 4.05 (d, $J_{6A,6A'}$ = 13.7 Hz, 1H, H-6A of CyD), 4.01 – 3.16 (m, 39H, Hs-2, Hs-3, Hs-4 and Hs-5 of CyD), 3.16 – 2.96 ppm (m, 2H, H-6A and H-6X of CyD). ^{13}C NMR (126 MHz, D_2O): δ 166.0 (C=O), 160.6 (C-3), 155.9 (C-17), 154.9 (C-19), 152.5 (C-5), 139.8 (C-6), 133.1 (C-21), 133.4 (C-9), 131.9 (C-15), 130.7 (C-23), 127.8 (C-8, C-10), 126.9 (C-13), 122.1 (C-7 and C-11), 120.0 (C-22 and C-14), 116.8 (C-16), 116.4 (C-20), 112.9 (C-12 and C-18), 102.3 (C-1G of CyD), 101.8 (Cs-1 of CyD), 101.4 (C-1A of CyD), 84.0 (C-4A of CyD), 80.3 (Cs-4 of CyD), 73.1-71.6 (Cs-2, Cs-3 and Cs-5 of CyD), 59.6 (Cs-6 of CyD), 41.1 ppm (C-6A of CyD). CD (H_2O) λ/nm (Δε): 211 (+1.4), 233 (-3.6), 275 (-1.7), 315 (+0.6). ESI-MS: m/z=1490.45 $[M+H]^+$. Analytical 8 minute Run. H_2O: Acetonitrile (95: 5 to 5: 95). RT = 2.59 minutes; purity = 100%. (Figure S26-28)

*Synthesis of 4-[3,5-bis(2-hydroxyphenyl)-1H-1,2,4-triazol-1-yl]-N-[3^A-deoxy-3^A-amino-β-cyclodextrin] benzamide (**2**)*

HOBt (24 mg, 0.175 mmol), DCC (36 mg, 0.175 mmol) were added to a solution of 3 (65.5 mg, 0.175 mmol) in dry DMF (5 mL). After 20 min, 3^A-amino-3^A-deoxy-β-cyclodextrin (199 mg, 0.175 mmol) was added. Reaction was stirred at room temperature under argon for 48 h. The solvent was evaporated to dryness in vacuo. The crude product was then triturated with diethyl ether (3 × 3 mL), followed by an acetone trituration cold (3 × 4 mL) and hot acetone trituration (3 × 3 mL) and the crude solids were purified by reverse phase chromatography using a 30g Biotage KP-RC-18 column (eluent: $H_2O \rightarrow CH_3OH$) to give the entitled product (white solid). For numbering of **2** refers to Figure 1. Yield: 57 % (149 mg, 0.10 mmol); TLC: Rf = 0.43 (iPrOH/AcOEt/H_2O/NH_3 4:3:2:1); ^{1}H NMR (500 MHz, D_2O): δ 7.94 (d, J = 7.7 Hz, 1H, H-13), 7.80 (bs, 2H, H-8 and H-10), 7.64–7.26 (m, 5H, H-7, H-11, H-15, H-21 and H-23), 7.14–6.95 (m, 3H, H-14, H-16 and H-22), 6.71 (s, 1H, H-20), 5.09 – 4.99 (m, 2H, Hs-1 of CyD), 4.97 (d, J = 3.4 Hz, 1H, H-1 of CyD), 4.85 (s, 2H, Hs-1 of CyD), 4.81 (s, 1H, H-1 of CyD), 4.59 (bs, 1H, H-1A of CyD), 4.46 – 2.78 (m, 42H, Hs-2, Hs-3, Hs-4, Hs-5 and Hs-6 of CyD).^{13}C NMR (126 MHz, d_6-DMSO): δ 165.4 (C=O), 160.2 (C-3), 156.8 (C-17), 155.7 (C-19), 152.4 (C-5), 140.2 (C-6), 134.6 (C-9), 132.9 (C-21), 131.8 (C-15), 131.4 (C-23), 128.8 (C-8, C-10), 127.1 (C-13), 123.6 (C-7 and C-11), 120.0 (C-22 and C-14), 117.5 (C-16), 116.6 (C-20), 114.9 (C-12), 114.1 (C-18), 104.6 (C-1A of CyD), 102.4-102.0 (Cs-1 of CyD), 82.4-81.0 (Cs-4 of CyD), 79.9 (C-5A of CyD), 73.6-71.2 (Cs-2, Cs-3 and Cs-5 of CyD), 60.7-60.0 (Cs-6 of CyD), 51.7 (C-3A). ESI-MS: m/z= 764.2 $[P+H+K]^{2+}$, 1490.45 $[M+H]$; CD (H_2O) λ/nm (Δε): 222 (+ 9.4), 233 (-10.2), 275 (-11.2), 315 (+4.5). Analytical 8 minute Run. H_2O: Acetonitrile (95: 5 to 5: 95). RT = 2.45 minutes; purity = 99%.

*Synthesis of 6^A-deoxy-6^A-[{(5-bromo-8-hydroxyquinolyl)-2-carboxyl}amino]-β-cyclodextrin (**5**)*

HOBt (22 mg, 0.16 mmol), DCC (33 mg, 0.16 mmol) and 5-bromo-8-hydroxyquinoline-2-carboxylic acid (Scheme S1) (43 mg, 0.16 mmol) were dissolved in anhydrous DMF (4.0 ml) under inert conditions. To this solution NEt_3 (45 µL, 0.32 mmol) was added followed by 6-monodeoxy-6-monoamino-β-cyclodextrin (187 mg, 0.16 mmol) added portion wise over 30 minutes at room temperature with vigorous stirring. The reaction mixture was stirred overnight under nitrogen. After 12 hours further addition of DCC (33 mg, 0.16 mmol), HOBt (22 mg, 0.16 mmol) and NEt_3 (22.5 µL, 1.0 eq) and heated at 50 °C for 5 days. Upon completion the reaction mixture was concentrated to dryness before trituration of the crude solid using diethyl ether (3 x 5 ml) was undertaken. The ether was decanted and the resulting solid was triturated using hot acetone (6 x 6 ml) and the solid product was dried by desiccation. The material was purified using reverse phase chromatography (30 g C18 Biotage Column) using liquid loading in H_2O: DMSO (1:2, 5 ml). The purification was run using a solvent system of H_2O: MeOH (100:0 – 0:100) yielding the pure final product **5** (124 mg, 56% yield, Rf = 0.5 (AcOEt: IPA: H_2O: NH_3 aq. (4: 3: 2: 1)). Analytical 8 minute run. H_2O: acetonitrile (70: 30 to 5: 95); RT = 1.84 minutes; purity = 100%. ^{1}H NMR (600 MHz, DMSO-d_6) δ 10.22 (s, 1H, NH), 9.53 (dd, J = 7.5, 4.4 Hz, 1H, OH of HQ), 8.57 (d, J = 8.7 Hz, 1H, H-3 of HQ), 8.24 (d, J = 8.7 Hz, 1H, H-4 of HQ), 7.86 (d, J = 8.3 Hz, 1H, H-6 of HQ), 7.10 (d, J = 8.3 Hz, 1H, H-7 of HQ), 5.94 (d, J = 6.0 Hz, 1H, OH of CyD), 5.86 (dd, J = 16.6, 6.4 Hz, 2H, OH of CyD), 5.75 (d, J = 11.4 Hz, 3H, OH of CyD), 5.72 – 5.65 (m, 6H, OH of CyD), 5.63 (s, 1H, OH of CyD), 5.51 (d, J = 7.5 Hz, 1H, OH of CyD), 4.98 (d, J = 3.7 Hz, 1H, H-1 of CyD), 4.84 (m, 3H, H-1 of CyD), 4.81 (d, J = 3.5 Hz, 1H, H-1 of CyD), 4.76 (d, J = 3.6 Hz, 1H, H-1 of CyD), 4.65 (d, J = 3.5 Hz, 1H, H-1 of CyD), 4.53 (s, 1H), 4.50 (s, 1H), 4.45 (s, 2H), 4.25 (s, 1H), 4.00 – 3.94 (m, 1H), 3.86 (dd, J = 12.3, 4.1 Hz, 1H), 3.81 (d, J = 11.2 Hz, 1H), 3.72 (d, J = 13.2 Hz, 1H), 3.69 (s, 1H), 3.72 – 3.66 (m, 1H), 3.68 – 3.60 (m, 8H), 3.63 – 3.59 (m, 2H), 3.57 (d, J = 11.4 Hz, 2H), 3.56 – 3.49 (m, 4H), 3.42 – 3.33 (m, 8H), 3.17 (t, J = 5.9 Hz, 1H), 2.56 – 2.50 (m, 1H). ^{13}C NMR (151 MHz, DMSO-d6) δ (ppm): 163.4 (C=O), 154.4 (C-8 of HQ), 148.6 (C-2 of HQ), 137.6 (C-4 of HQ), 137.2 (C-9 of HQ), 133.1 (C-6 of HQ), 128.4 (C-10 of HQ), 120.8 (C-3 of HQ), 113.0 (C-7 of HQ), 108.7 (C-5 of HQ), 102.7 (C-1 of CyD), 102.7(C-1 of CyD), 102.6 (C-1 of CyD), 102.3 (C-1 of CyD), 102.1 (C-1 of CyD), 101.5 (C-1 of CyD), 85.03 (C-4A of CyD), 82.3-80.9 (Cs-4 of CyD),

74.2-70.5 (Cs-3, Cs-5, Cs-2 of CyD), 60.5 (C-6 of CyD), 60.3 (C-6 of CyD), 60.2 (C-6 of CyD), 60.1 (C-6 of CyD), 59.6 (C-6 of CyD), 58.9 (C-6 of CyD), 40.6 (C-6A of CyD). HRMS: m/z= 1405.3227 $[M+Na]^+$. Analytical 8 minute run; H_2O: acetonitrile (70: 30 to 5: 95); RT = 1.84 minutes; purity =100%.

NMR spectroscopy and MS spectrometry

^1H and ^{13}C NMR spectra were recorded at 25 °C with a Varian UNITY PLUS-500 spectrometer at 499.9 and 126 MHz, respectively. The NMR spectra were obtained by using standard pulse programs from the Varian library. The 2D experiments (COSY, TOCSY, gHSQCAD, gHMBC, ROESY) were acquired by using 1000 data points, 256 increments, and a relaxation delay of 1.2 s. The spectra were referred to as the solvent signal.

UV-visible and circular dichroism spectroscopy

UV spectra were recorded on an Agilent 8452A diode array spectrophotometer. Circular dichroism measurements were performed on a JASCO spectropolarimeter (model J-1500).

Iron stability constants determination

The automated titration system consists of a Metrohm Dosimat 765 liter ml syringe, a Mettler Toledo MP230 pH meter with SENTEK pH electrode (P11), and an HP 8453 UV-visible spectrophotometer with a Hellem quartz flow cuvette being circulated through by a Gilson Mini-plus #3 pump — speed capability (20 mL/min). A potassium chloride electrolyte solution (0.1 mol/L) was used to maintain the ionic strength. The temperature of the test solutions was maintained in a thermostatic jacketed titration vessel at 25 °C (± 0.1 °C) using a Fisherbrand Isotemp water bath. The pH electrodes were calibrated using GLEE[41] with data obtained by titrating a volumetric standard HCl (0.1 mol/L) in KCl (0.1 mol/L) with KOH (0.1 mol/L) under an argon gas atmosphere in the vessel. The solution under investigation was stirred vigorously during the experiment. For pKa determinations, a cuvette path length of 10 mm was used while for metal stability constant determinations, a cuvette path length of 50 mm was used. All instruments were interfaced to a computer and controlled by an in-house program. An automated titration adopted the following strategy: the pH of a solution was increased by 0.1 pH unit by the addition of potassium hydroxide solution (0.1 mol/L) from the autoburette. The pH readings were judged to be stable if their values varied by less than 0.01 pH unit after a set incubation period. For pKa determinations, an incubation period of 1.5 mins was adopted; for metal stability, constant determinations, an incubation period of 3 mins was adopted. The cycle was repeated until the defined end point pH value was achieved. Titrations were carried out in the solution with a molar ratio of DMSO: H_2O being 0.2: 1 due to the solubility issue of the three analogs and/or corresponding iron-complexes. Under this condition, the pH meter readings are shifted, compared to the aqueous solution. All the titration data were analyzed with the HypSpec2014 program[42,43] (http://www.hyperquad.co.uk/). The speciation plot was calculated with the HYSS program.[44] Analytical grade reagent materials were used in the preparation of all solutions.

Dynamic light scattering measurements

Dynamic light-scattering (DLS) measurements were carried out using a Zetasizer Nano ZS (Malvern Instruments, UK) equipped for backscattering at 173° with a 633 nm He–Ne laser. Each DLS measurement was run using automated, optimal measurement times, and laser attenuation settings according to literature.[31]

Trolox Equivalent Antioxidant Capacity Assay

In vitro, antioxidant assays were performed by 2,2'-azinobis(3-ethylbenzothiazoline-6-sulfonic acid) diammonium salt ($ABTS^{\bullet+}$) radical cation decolorization assay using 6-hydroxy-2,5,7,8-tetramethylchroman-2-carboxylic acid (Trolox) as reported elsewhere.[45] In brief, the radical cation $ABTS^{+\cdot}$ was generated by a reaction between ABTS (7 mM) and persulphate (2.45 mM) in water for 16 h (dark, room temperature). This radical solution was diluted in phosphate buffer (10 mM, pH 7.4) and combined with different concentrations of the sample antioxidants (**1**, **2** and **3**). All samples were diluted approximately to provide 20–80% inhibition of the blank absorbance. The absorbance values were measured for 6 min. Solution absorbance was plotted vs. test compound concentration; each resultant slope was normalized concerning that obtained for Trolox to give the Trolox-equivalence (TEAC) value for each time point (1, 3, 6 min). All measurements were performed in triplicate.

Anti-aggregation assay.

αSyn solutions (0.5 mg/mL) were buffered at pH 6.6 and 7.4 (MOPS, 20 mM). Iron and copper-mediated aggregation of αSyn was studied using suitable $FeCl_3$ and $Cu(ClO_4)_2$ solutions in order to have a final concentration of 265 μM in cuvette as reported elsewhere. CyD derivatives were added in an equimolar amount to the copper ions.[31] Each DLS measurement was run by using automated, optimal measurement times, and laser attenuation settings.

Cell Lines

WT and Npc1-/- null CHO cells were used (Isolation of NPC1-Deficient Chinese Hamster Ovary Cell Mutants by Gene Trap Mutagenesis.[46]

LysoTracker Green and Propium Iodide staining

In vitro FACs experiment were done in order to measure the acidic compartment volumes according to the published method.[47] Live cells were stained with LysoTracker™ Green DND-26 (Thermo Fisher-L7526) at 250 nM for 10 min in PBS at RT, centrifuged at 1200x, 10 min and cells resuspended in FACs buffer (PBS, 1% BSA, 0.1% NaN_3 sodium azide). Cells were stained with Propidium Iodide (20 nM) (Invitrogen-P3566) immediately before analysis on the FACs machine for dead cell separation. FACs analyses were performed with 10.000-recorded cells by using FACs Canto with BD software.

Acknowledgments

We thank Professor Robert Hider (Kings College) for useful discussions and help with the iron measurements. The Niemann Pick Research Foundation are thanked for continued financial support (JMG, EK, AM, FMP, JS). The authors are also grateful for support from Università degli Studi di Catania (Piano della Ricerca di Ateneo 2016-2018) and the Italian Ministero dell'Università e della Ricerca (VO, GV). FMP is a Wellcome Trust Investigator in Science.

Keywords: deferasirox • Niemann-Pick • Iron complexes • protein aggregation • antioxidant

[1] P. Delangle, E. Mintz, *Dalton Trans.* **2012**, *41*, 6359-6370.
[2] T. Zhou, Y. Ma, X. Kong, R. C. Hider, *Dalton Trans.* **2012**, *41*, 6371-6389.
[3] M. G. Savelieff, G. Nam, J. Kang, H. J. Lee, M. Lee, M. H. Lim, *Chem. Rev.* **2019**, *119*, 1221–1322.
[4] R. J. Ward, D. T. Dexter, R. Crichton, *Curr. Med. Chem.* **2012**, *19*, 2760-2772.
[5] J. J. Meerpohl, G. Antes, G. Rücker, N. Fleeman, E. Motschall, C. M. Niemeyer, D. Bassler, *Cochrane Database Syst. Rev.* **2012**, 2.

[6] M. A. Santos, S. M. Marques, S. Chaves, *Coord. Chem. Rev.* **2012**, *256*, 240-259.
[7] V. M. Nurchi, G. Crisponi, J. I. Lachowicz, S. Medici, M. Peana, M. A. Zoroddu, *J. Trace Elem. Med. Biol.* **2016**, *38*, 10-18.
[8] M. Marano, G. Bottaro, B. Goffredo, F. Stoppa, M. Pisani, A. M. Marinaro, F. S. Falvella, *Eur. J. Clin. Pharm.* **2016**, *72*, 247.
[9] J. D. Díaz-García, A. Gallegos-Villalobos, L. Gonzalez-Espinoza, M. D. Sanchez-Nino, J. Villarrubia, A. Ortiz, *Nat. Rev. Nephr.* **2014**, *10*, 574.
[10] P. Rouge, M. Becuwe, A. Dassonville-Klimpt, S. Da Nascimento, J. F. Raimbert, D. Cailleu, P. Sonnet, *Tetrahedron* **2011**, *67*, 2916-2924.
[11] P. M. Dandagi, S. L. Adavi, S. Rath, A. P. Gadad, *Int. J. Pharm. Sci.* **2014**, *6*, suppl. 2, 251-256.
[12] A. Puglisi, J. Spencer, V. Oliveri, G. Vecchio, X. Kong, J. Clarke, J. Milton, *Dalton Trans.* **2012**, *41*, 2877-2883.
[13] V. Oliveri, F. Attanasio, A. Puglisi, J. Spencer, C. Sgarlata, G. Vecchio, *Chem.– Eur. J.* **2014**, *20*, 8954-8964.
[14] V. Oliveri, A. Puglisi, M. Viale, C. Aiello, C. Sgarlata, G. Vecchio, J. Clarke, J. Milton and J. Spencer, *Chem.-Eur. J.* **2013** *19* 13946–13955.
[15] V. Oliveri, F. Bellia, G. Vecchio, *Chem.-Eur. J.* **2017**, *23*, 4442-4449.
[16] T. Serno, R. Geidobler, G. Winter, *Adv. Drug Deliv. Rev.* **2011**, *63*, 1086-1106.
[17] V. Oliveri, G. Vecchio, *Chem.–Asian J.* **2016**, *11*, 1648-1657.
[18] P. Bar-On, E. Rockenstein, A. Adame, G. Ho, M. Hashimoto, E. Masliah, *J. Neurochem.* **2006**, *98*, 1032-1045.
[19] S. Kaewprasert, M. Okada, Y. Aoyama, *J. Nutr Biochem.* **2002**, *13*, 219-225.
[20] E. Barone, F. Di Domenico, D. A. Butterfield, *Biochem. Pharmacol.* **2014**, *88*, 605-616.
[21] C. Coisne, S. Tilloy, E. Monflier, D. Wils, L. Fenart, F. Gosselet, *Molecules* **2016**, *21*, 1748-1770.
[22] A. Schlatter, W. D. Woggon, *Adv. Synth. Catal.* **2008**, *350*, 995-1000.
[23] C. M. Pedersen and M. Bols, in *Organic Synthesis and Molecular Engineering*, John Wiley & Sons, Inc., Hoboken, NJ, USA, **2013**, pp. 305–332.
[24] V. Oliveri, A. Pietropaolo, C. Sgarlata, G. Vecchio, *Chem.–Asian J.* **2017**, *12*, 110-115.
[25] V. Oliveri, F. Bellia, A. Pietropaolo, G. Vecchio, *Chem.-Eur. J.* **2015**, *21*, 14047-14059.
[26] M. Kodaka, *J. Phys. Chem.* **1991**, *95*, 2110-2112.
[27] S. Steinhauser, U. Heinz, M. Bartholomä, T. Weyhermüller, H. Nick, K. Hegetschweiler, *Eur. J. Inorg. Chem.* **2004**, 4177-4192.
[28] U. Heinz, K. Hegetschweiler, P. Acklin, B. Faller, R. Lattmann, H. P. Schnebli, *Angew. Chemie Int. Ed.* **1999**, *38*, 2568-2570.
[29] K. Jomova, M.Valko, *Curr. Pharm. Des.* **2011**, *17*, 3460-3473.
[30] E. Niedzielska, I. Smaga, M. Gawlik, A. Moniczewski, P. Stankowicz, J. Pera, M. Filip, *Mol. Neurobiol.* **2015**, 1-32.
[31] S. Ojha, H. Javed, S. Azimullah, M. E. Haque, *Mol. Cell. Biochem.* **2016**, *418*, 59-70.
[32] J. J. Sutachan, Z. Casas, S. L. Albarracin, B. R. Stab, I. Samudio, J. Gonzalez, G. E. Barreto, *Nutr. Neurosci.* **2012**, *15*, 120-126.
[33] A. Aguzzi, T. O'Connor, *Nat. Rev. Drug Discov.* **2010**, *9*, 237-248.
[34] E. A. Waxman, B. I. Giasson, *Biochim. Biophys. Acta (BBA)-Mol. Basis Dis.* **2009**, *1792*, 616-624.
[35] V. Oliveri, *Eur. J. Med. Chem.* **2019**, *167*, 10-36.
[36] A. Dusa, J. Kaylor, S. Edridge, N. Bodner, D. P. Hong, A. L. Fink, *Biochemistry* **2006**, *45*, 2752-2760.
[37] V. Oliveri, C. Sgarlata, G. Vecchio, *Chem.-Asian J.* **2016**, *11*, 2436-2442.
[38] S. Steinhauser, U. Heinz, J. Sander, K. *Z.* Hegetschweiler, *Anorg. Allg. Chem.* **2004**, *630*, 1829-1838.
[39] V. Oliveri, S. Zimbone, M. L. Giuffrida, F. Bellia, M. F. Tomasello, G. Vecchio, *Chem.-Eur. J.* **2018**, *24*, 6349-6353.
[40] A. Puglisi, J. Spencer, J. Clarke, J. Milton, *J. Inclus. Phenom. Macrocyclic Chem.* **2012**, *73*, 475-478.
[41] P. Gans, B. O'Sullivan, *Talanta* **2000**, *51*, 33-37.
[42] P. Gans, A. Sabatini, A. Vacca, *Annali di chimica* **1999**, *89*, 45-49.
[43] P. Gans, A. Sabatini, A. Vacca, *Talanta* **1996**, *43*, 1739-1753.
[44] L. Alderighi, P. Gans, A. Ienco, D. Peters, A. Sabatini, A. Vacca, *Coord. Chem. Rev.* **1999**, 184, 311-318.
[45] C. Sgarlata, V. Oliveri, J. Spencer, *Eur. J. Inorg. Chem.* **2015**, 5886-5891.
[46] K. Higaki, H. Ninomiya, Y. Sugimoto, T. Suzuki, M. Taniguchi, H. Niwa, P.G. Pentchev, M.T. Vanier, K. Ohno, *J. Biochem.* **2001**, *129*, 875–880.
[47] D. Te Vruchte, A.O. Speak, K.L. Wallom, N. Al Eisa, D. A. Smith, C. J. Hendriksz, L. Simmons, R. H. Lachmann, A. Cousins, R. Hartung, E. Mengel, H. Runz, M. Beck, Y. Amraoui, J. Imrie, E. Jacklin, K. Riddick, N. M. Yanjanin, C. A. Wassif, A. Rolfs, F. Rimmele, N. Wright, C. Taylor, U. Ramaswami, T. M. Cox, C. Hastings, X. Jiang, R. Sidhu, D. S. Ory, B. Arias, M. Jeyakumar, D. J. Sillence, J. E. Wraith, F. D. Porter, M. Cortina-Borja, F. M. Platt, *J. Clin. Invest*. **2014**, *124*, 1320-1328.

Entry for the Table of Contents
Layout 1:

FULL PAPER

We conjugated deferasirox with β-cyclodextrin creating hybrid non-toxic molecules with multiple biological properties.

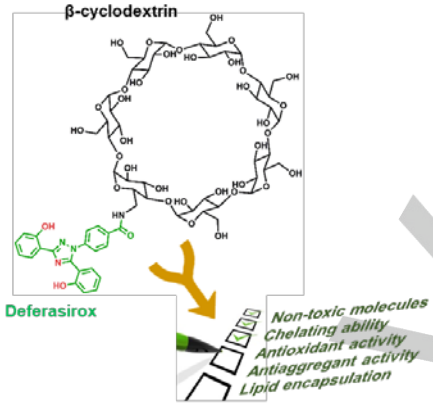

Jose Miguel Gascon, Valentina Oliveri, Andrew McGown, Ecem Kaya, Yu-Lin Chen, Carol Austin, Martin Walker, Frances Platt,* Graziella Vecchio,* and John Spencer **

Page No. – Page No.

Synthesis and Study of Novel Multifunctional Cyclodextrin-Deferasirox Hybrids